Journal of ELECTRONIC MATERIALS, Vol. 45, No. 6, 2016
DOI: 10.1007/s11664-015-4310-7

Intrinsic Doping in Electrodeposited ZnS Thin Films for Application in Large-Area Optoelectronic Devices

MOHAMMAD LAMIDO MADUGU,[1,3] OLAJIDE IBUKUN-OLU OLUSOLA,[1] OBI KINGSLEY ECHENDU,[1,2] BURAK KADEM,[1] and IMYHAMY MUDIY DHARMADASA[1]

1.—Materials and Engineering Research Institute, Sheffield Hallam University, Sheffield S1 1WB, UK. 2.—Department of Physics, Faculty of Science, Federal University of Technology, Owerri, Nigeria. 3.—e-mail: maduguu@yahoo.com

Zinc sulphide (ZnS) thin films with both *n*- and *p*-type electrical conductivity were grown on glass/fluorine-doped tin oxide-conducting substrates from acidic and aqueous solution containing $ZnSO_4$ and $(NH_4)_2S_2O_3$ by simply changing the deposition potential in a two-electrode cell configuration. After deposition, the films were characterised using various analytical techniques. X-ray diffraction analysis reveals that the materials are amorphous even after heat treatment. Optical properties (transmittance, absorbance and optical bandgap) of the films were studied. The bandgaps of the films were found to be in the range (3.68–3.86) eV depending on the growth voltage. Photoelectrochemical cell measurements show both *n*- and *p*-type electrical conductivity for the films depending on the growth voltage. Scanning electron microscopy shows material clusters on the surface with no significant change after heat treatment at different temperatures. Atomic force microscopy shows that the surface roughness of these materials remain fairly constant reducing only from 18 nm to 17 nm after heat treatment. Thickness estimation of the films was also carried out using theoretical and experimental methods. Direct current conductivity measurements on both as-deposited and annealed films show that resistivity increased after heat treatment.

Key words: *n*-Type and *p*-type ZnS, thin film, electrodeposition, intrinsic doping, amorphous

INTRODUCTION

Zinc sulphide (ZnS) is an important wide bandgap II–VI semiconductor material with a direct optical bandgap of 3.70 eV.[1] This bandgap is convenient when used as a window material in solar cells, since it allows for high transparency in the short wavelength region (350–550) nm when compared to CdS with a bandgap of 2.42 eV. ZnS has a refractive index (n) of 2.40 which also makes it possible for application as antireflective coatings in thin-film solar cells.[2] This material is under intense study and has gained application in the areas of solar cells[3,4] and various photonic devices.[5]

(Received August 5, 2015; accepted December 16, 2015; published online January 5, 2016)

ZnS can be *n*- or *p*-type[6] in electrical conduction depending on the growth conditions. This material usually grows in zinc blende and/or wurtzite crystal structures which, in both cases, show a direct optical energy gap.[7] ZnS with either *n*- or *p*-type electrical conduction is important especially in the fabrication of solar cells and other electronic devices. The incorporation of chemical bath-deposited (CBD) ZnS as a buffer/window has yielded an efficiency of 18.6% in ZnS/Cu(In,Ga)Se_2 solar cells comparable to 19.9% efficiency achieved using CdS.[2] Echendu et al.[3] incorporated *n*-type ZnS as a window layer in a ZnS/CdTe solar cell, achieving 12% efficiency. Han et al.[8] used ZnS in a ZnS/CdS/CdTe solar cell structure with a conversion efficiency of over 10%. Pudov et al.[9] used CBD-ZnS as a window layer in a copper indium gallium diselenide

(CIGS)-based solar cell and achieved a conversion efficiency of over 18.0%. The effort to substitute the well-known CdS, which is so far the best partner to CdTe in the CdS/CdTe solar cell structure with a wider bandgap material like ZnS, is on course so that conversion efficiency can be further improved.

ZnS thin films have been grown using different techniques such as CBD,[10] successive ionic layer adsorption and reaction (SILAR),[11] spray pyrolysis[12] and electrodeposition.[5] In the present work, potentiostatic electrodeposition using a simple two-electrode system was employed to deposit electronic device-quality ZnS thin films from aqueous electrolyte containing $ZnSO_4$ and $(NH_4)_2S_2O_3$. The strengths of this technique include its simplicity, intrinsic doping, a low cost, low-temperature processing, low chemical waste generation and application in large-area optoelectronics.

The ability to grow a particular semiconductor with both *n*- and *p*-type electrical conductivity makes it applicable in various functions in electronic devices. ZnS thin films have been grown by many researchers using different techniques, as mentioned above. Bhalerao et al.[13] electrodeposited *n*-type ZnS on a stainless steel substrate. Falcony et al.[12] deposited ZnS:Mn on a Pyrex glass substrate using spray pyrolysis, and Peng et al.[14] deposited *n*-type ZnS to improve the performance of their organic light emitting diodes (OLEDs). Echendu et al.[6] electrodeposited both *n*-type and *p*-type ZnS films on glass/fluorine-doped tin oxide (glass/FTO) substrates from two separate electrolytes by varying the [Zn]/[S] ratio.

In the present work, ZnS thin films of both *n*- and *p*-type electrical conductivity have been electrochemically synthesised using only one electrolyte and a two-electrode cell by simply changing the deposition potential. This doping is achieved, therefore, by a compositional change within the material layer.

EXPERIMENTAL PROCEDURE

ZnS thin films were deposited from acidic and aqueous solution containing 0.15 M $ZnSO_4$ of a purity of 5 N (99.999%) and 0.15 M $(NH_4)_2S_2O_3$ of 98% purity in 400 mL of deionised water using a potentiostatic electrodeposition method in a two-electrode cell configuration. All chemicals and the glass/FTO substrate were purchased from Sigma-Aldrich Ltd. (UK). The pH of the bath was adjusted to 4.00 ± 0.02 using dilute sulphuric acid (H_2SO_4) and the deposition temperature was ~30°C. The decision to stay with growth temperature of 30°C is due to precipitation in the electrolyte at higher temperatures. Precipitation starts to form at growth temperature of ~50°C which turns the electrolyte cloudy with undissolved particles settling at the bottom of the bath. Observation has also shown that this precipitation leads to instability in the pH of the electrolyte; hence, our decision to stay with 30°C at which the electrolyte is clear and stable. The glass/FTO served as the cathode while the anode was a high-purity carbon rod. Pre-deposition cleaning of the substrates was done using soap solution and methanol to remove grease and then rinsing in deionised water. The electroplating work was carried out using a computerised Gill AC potentiostat system. The source of heat and stirring was a hot plate with a magnetic stirrer, and the stirring rate of the bath was moderately maintained throughout the deposition. The substrates were attached to a graphite rod using polytetraethylene (PTFE) tapes before insertion into the deposition electrolyte. The two electrodes (cathode and anode) were held vertically and stationary in the deposition electrolyte throughout the deposition period. After growth, the layers were subjected to various characterisation techniques [x-ray diffraction (XRD), photoelectrochemical (PEC) cell, optical absorption, scanning electron microscopy (SEM), atomic force microscopy (AFM), and Raman and Direct current conductivity measurements] in order to optimise the growth conditions for high-quality ZnS layers for application in thin-film solar cells.

DEPOSITION OF ZNS LAYERS

Before deposition, a cyclic voltammogram of the deposition electrolyte containing both Zn^{2+} and S^{2-} ions was taken in order to find the approximate deposition potential range for ZnS. The deposition of ZnS films on the cathode is given by the following electrochemical equation.

$$Zn^{+2} + 2e^- + S \rightarrow ZnS. \quad (1)$$

Figure 1 shows a typical cyclic voltammogram of an aqueous electrolyte containing 0.15-M $ZnSO_4$ + 0.15-M $(NH_4)_2S_2O_3$ at ~30°C using glass/FTO substrate. The voltammogram was run at a cathodic potential range of (0–2000) mV and the scan rate was 3 mV s^{-1}.

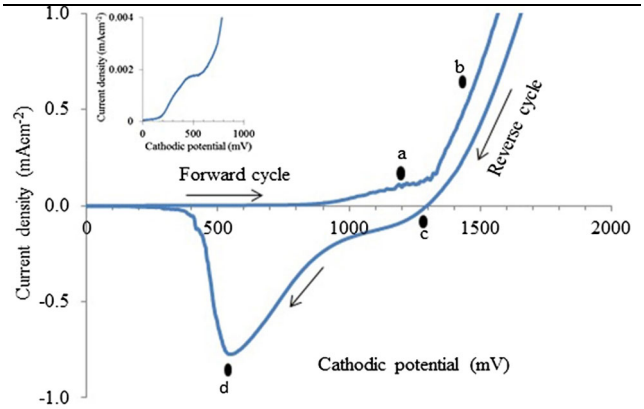

Fig. 1. Cyclic voltammogram of the aqueous solution containing 0.15-M $ZnSO_4$ + 0.15-M $(NH_4)_2S_2O_3$ in 400 mL of deionised water. Both the growth temperature and the pH were set to ~30°C and 4.00 ± 0.02, respectively.

Sulphur (S) with low reduction potential of E^0 = + 0.449 V starts to deposit immediately at the beginning of the deposition, as revealed by the inset diagram of Fig. 1, during the forward cycle. The deposition of sulphur continues while zinc (Zn) with reduction potential of −0.762 V is expected to start depositing after 1000 mV around point ***a***. At a certain voltage around 1450 mV, stoichiometric ZnS films are deposited. From point ***b*** and above, Zn rich ZnS is deposited due to an increase in cathodic voltage which influences more *n*-type doping. This is observed from the PEC cell measurement plot in Fig. 2. The deposition window for ZnS is, therefore, (1200–1650) mV depending on whether S-rich ZnS or Zn-rich ZnS is desired. In the reverse cycle, two negative peaks at points ***c*** (∼1300 mV) and ***d*** (∼550 mV) represent the dissolution of Zn and S, respectively.

Photoelectrochemical (PEC) Cell Studies

The PEC cell study was carried out to determine the electrical conductivity type of the films in both as-deposited and heat-treated conditions. The electrolyte used in this study was 0.10-M $Na_2S_2O_3$ in 20 mL of deionised water. When the glass/FTO/ZnS films are immersed in the electrolyte, a solid/liquid junction is formed between the ZnS thin film and the electrolyte (junction diagram not shown for brevity). Dharmadasa et al.[15] also used a similar set-up with KI electrolyte to determine the electrical conductivity type of their electrodeposited ZnSe layers in which they show the similarity of the solid/liquid junction to a Schottky barrier junction. Similar configuration with 1.0-M polysulphide electrolyte was used by Bhalerao et al.[13] to determine the PEC signal of their photoelectrochemical cell-based electrodeposited layers. Depending on the electrical conductivity type of the substrate, band bending takes place at the semiconductor/liquid interface. This results in the formation of a depletion region within the semiconductor material. The difference between the voltage under illumination (V_L) and dark (V_D) condition gives the PEC signal produced by the solid/liquid junction. Prior to the measurements, the system was calibrated with a known *n*-type (CdS) material. Positive PEC signal indicates *p*-type electrical conductivity whereas negative PEC signal indicates *n*-type electrical conductivity. The magnitude of the PEC signal is indicative of the doping concentration of the semiconductor under study. This is an easy and quick way to check the electrical conductivity type of semiconductor materials especially when they are grown on conducting substrates.

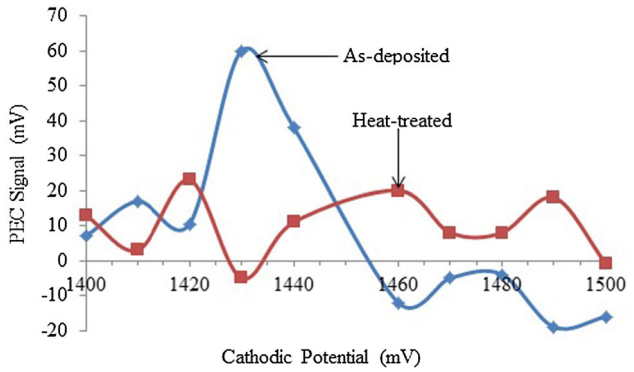

Fig. 2. PEC cell measurement for both as-deposited and heat-treated ZnS layers.

Figure 2 shows the PEC signal versus cathodic potential for ZnS samples grown at different growth voltages ranging from (1400 to 1500) mV.

For the as-deposited samples, it was observed that at low cathodic deposition potentials, the material is *p*-type due to S-richness, and at higher cathodic deposition potential, the material is *n*-type due to Zn-richness which shows intrinsic doping. The transition point from *p*- to *n*-type is where the stoichiometric material is obtained with equal amounts of Zn and S in the layer. This point may shift by a few millivolts (mV) in either direction from time to time due to bath replenishment with either Zn^{2+} or S^{2-} ions. However, this point is important as it serves as the reference point for the grower. After deposition, heat treatment is usually done to improve the structural, optical and electronic properties of the semiconductor materials for device application. The low PEC signals observed for the samples (generally <100 mV) in this work relative to other semiconductor materials could be due to the wide bandgap nature of ZnS which induces it to transmit most of the visible light. A similar conclusion was also drawn by Bhalerao et al.[13] For the heat-treated samples, almost all the materials become *p*-type due to stoichiometry adjustment brought about by the heat-treatment process.

The achievement of both *n*- and *p*-type ZnS films in this work is due to stoichiometric deviation. These deviations were achieved due to variation in the cathodic potential as shown in the PEC cell measurement (Fig. 2). The two semiconductor elements involved in this deposition electrolyte are sulphur (with reduction potential E^0 = + 0.449 V) and Zn (with reduction potential E^0 = −0.762 V). At low potentials, sulphur with a more positive reduction potential is first deposited due to its more positive E^0 value while Zn will deposit at higher cathodic potentials. Films grown at low cathodic potentials are *p*-type due to S-richness while those grown at higher cathodic potentials are *n*-type due to Zn-richness. Increases in the cathodic potential incorporates more Zn to the layer, thereby increasing the *n*-type doping of the material, while a decrease in the cathodic potential results in incorporation of more S, thereby doping the material to a *p*-type material. Between these two regions, there is an inversion point where material changes either from *p*- to *n*-type or *n*- to *p*-type in electrical conduction around 1450 mV. The layers grown in

the vicinity of this voltage show intrinsic behaviour with low electrical conduction and the Fermi level is expected to be in the middle. The achievement of both *n*-type and *p*-type thin films of ZnS in this work have to do with the variation of the material composition. In other words, this is doping by composition. The supply of free electrons, Zn atoms in these layers grown from these two regions are different and are responsible for the change in electrical conduction type.[16] Even though the material is amorphous, the concentration of Zn atoms, the free electron supplier, decides whether the layer is *p*- or *n*-type in electrical conduction.

X-ray Diffraction

XRD patterns were carried out to study the structure of electroplated thin film ZnS layers using a Philips PW 3710 X' pert Pro diffractometer employing a Cu-K_α radiation source (λ = 1.542 Å). The scans were carried out in the range 2θ = (20–70)°.

Figure 3 shows the XRD patterns for the as-deposited and heat-treated ZnS layers grown at different cathodic potentials.

It can be observed that there are no XRD peaks due to ZnS layers. All the peaks are due to the glass/FTO substrate even after heat treatment at 350°C for 15 min in air. This result shows that the ZnS layers are amorphous in nature based on the growth conditions used. A similar result was also obtained by Echendu et al.[5,6] However, where the material is polycrystalline, as reported by Refs. 2, 17, and 18, irrespective of the growth technique, the layers show a preferential orientation along the (111) cubic phase of the ZnS peak at around 2θ = 30°. This peak is missing in the XRD pattern shown in Fig. 3a and b.

Raman Spectroscopy

Raman spectroscopy is a technique that gives information on the molecular vibration and other structural properties like crystallinity and phases of materials. In this work, the Raman excitation energy source was a green laser (λ = 514 nm). Figure 4 shows the Raman spectra of ZnS thin films grown on glass/FTO substrate at room temperature.

Observed from the spectra are two broad peaks at 147 cm^{-1} and 217 cm^{-1} identified as 2TA and 2LA optical mode phonons for ZnS, respectively.[19] The broad nature of these peaks complements the XRD which revealed that this material is amorphous. It can be observed in the as-deposited condition that the material shows an amorphous behaviour with virtually no peaks. However, after heat treatment, an improvement with emergence of a small broad peak at 217 cm^{-1} was observed.

Optical Absorption

Optical properties of semiconductors intended for use in optoelectronics devices like solar cells are important and useful properties critical to the device performance. These properties indicate the suitability of a particular material for a particular application. The optical properties of glass/FTO/ZnS films were investigated using a Cary 50 ultraviolet–visible light (UV–Vis) spectrophotometer at room temperature. A bare glass/FTO substrate was used

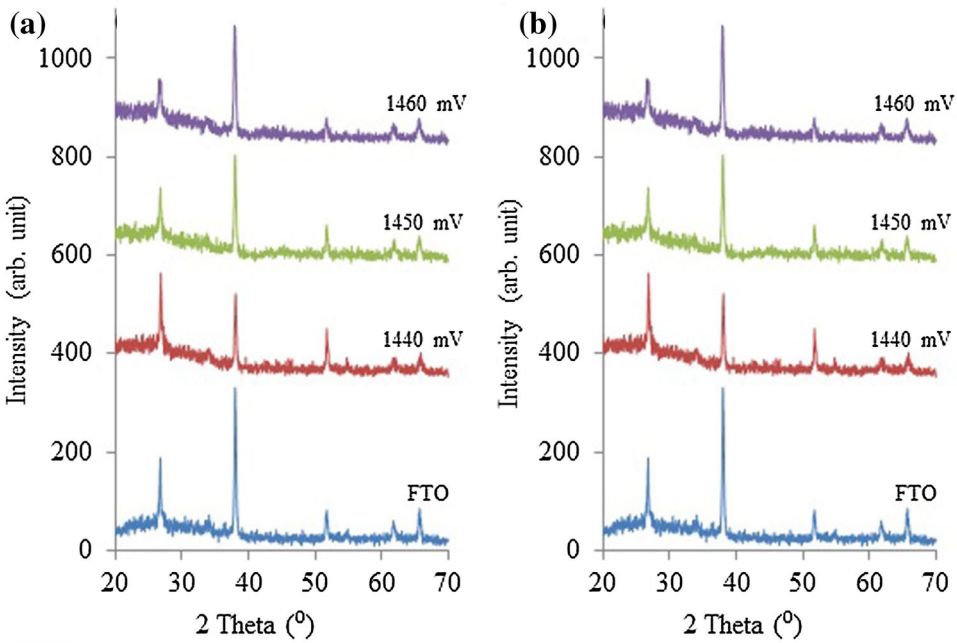

Fig. 3. XRD patterns of ZnS layers grown on glass/FTO substrate at different cathodic potentials for (a) as-deposited and (b) heat-treated (at 350°C for 15 min in air) layers.

as a reference before performing the optical measurements on the glass/FTO/ZnS substrates. Important optical properties studied include transmittance, absorbance and optical bandgap of the thin films; this is shown in Fig. 5.

Figure 5a shows the transmittance spectra of ZnS thin films grown at 1400 mV, 1450 mV and 1500 mV. The film grown at 1400 mV shows higher transmittance in the range of 80–90% in the visible region of the solar spectrum while the films grown at 1450 mV and 1500 mV show transmittance in the range of 45–70% in the visible spectrum. Observation shows that, the transmittance of the films decrease with increase in growth voltage. One quality of a good buffer/window layer is to have high transmittance and minimal absorption.

Figure 5b shows that the absorbance of the films decreases with a decrease in the growth voltage; a strong absorbance is observed at a cathodic potential of 1500 mV. Figure 5c shows the optical bandgap energy for the same ZnS thin films. The energy bandgap is obtained by extrapolating the straight line portion of the absorption ($A^2 = 0$) to the energy axis.[20] Looking at this figure, the energy bandgaps of these films are found to be 3.86 eV, 3.72 eV and 3.68 eV for films grown at 1400 mV, 1450 mV and 1500 mV, respectively. It is observed that the bandgap energy decreases with an increase in growth voltage. The highest bandgap of 3.86 eV obtained for these films was grown at 1400 mV, corresponding to the film with highest transmittance. The bandgaps obtained for the other two films decrease as the growth voltage is increased, corresponding to low transmittance seen in Fig. 5a. This shows that increase in growth voltage results in the increase in Zn content in the film reducing the light transmission and the energy bandgap value.

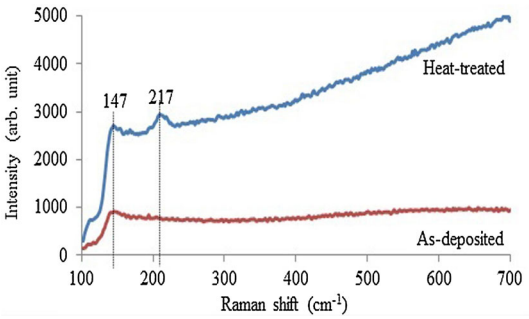

Fig. 4. Typical Raman scattering spectra recorded on glass/FTO/ZnS thin films of as-deposited and heat-treated (at 350°C for 15 min in air) samples.

Scanning Electron Microscopy (SEM)

SEM micrographs of the glass/FTO/ZnS films were determined using an FEI 200 Nova nano SEM instrument using 10.0-kV electron beam voltage with magnification of 60,000× for the as-deposited and heat-treated layers (at different heat-treatment temperatures). The SEM was carried out to study the morphology and the effects of different heat treatment on the surface morphology of the ZnS films. Figure 6 shows SEM images of glass/FTO/ZnS substrates.

All layers were grown at a cathodic potential of ~1450 mV to achieve stoichiometric ZnS thin films and were then heat-treated at different temperatures of 100°C, 200°C and 300°C for 15 min in air. Heat treatment above 300°C was avoided in order not to deteriorate the material. The film morphology shows a fairly uniform coverage of the glass/FTO substrate. The heat treatment at different temperatures was done to study the trend in the effects of heat treatment on the surface morphology of the films. However, closed observation shows that there is no significant improvement upon annealing of the morphology of the films. This further confirms the amorphous nature of these materials.

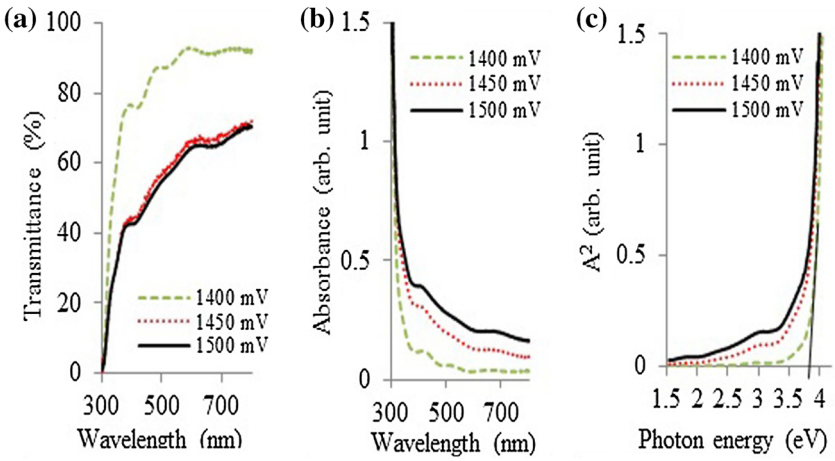

Fig. 5. (a) Transmittance (b) absorbance and (c) optical bandgap of heat-treated ZnS thin films deposited at different growth voltages.

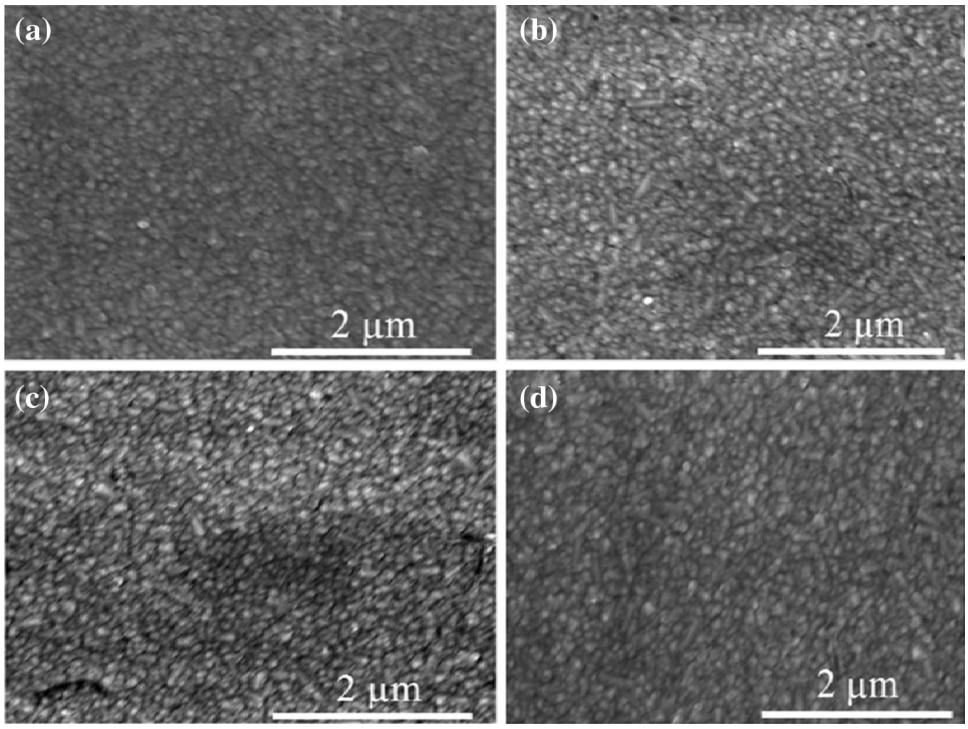

Fig. 6. SEM images for (a) as-deposited and (b), (c), and (d) for heat-treated glass/FTO/ZnS layers at 100°C, 200°C and 300°C, respectively for 15 min in air. The layer was grown at 1450 mV to obtain a thickness of ~880 nm.

Atomic Force Microscopy (AFM) Studies

AFM studies were carried out to determine the surface topographies of the ZnS thin films under study. This measurement was carried out using a Burke nanoscope IIIa multimode AFM instrument. Figure 7a and b show the AFM images of as-deposited and heat-treated glass/FTO/ZnS layers.

Figure 7a and b shows the two-dimensional (2D) and three-dimensional (3D) AFM images for as-deposited and heat-treated films, respectively. A small decrease in surface roughness after heat treatment was observed. The average surface roughness of this material is estimated to be ~18 nm in the as-deposited layers and reduced to ~17 nm after heat treatment. The roughness in thin films could be due to the nature of the substrate used. In the electrodeposition growth method, the films usually start to nucleate at the spiky tips of the FTO owing to a high electric field at these points; this is due to the nature of the technique and the morphology of FTO surface, since the growth method is electric field-driven. To eliminate or reduce surface roughness and pinholes in thin films, substrates with low surface roughness should be used. This is important since surface roughness affects device performance and may even lead to pinholes which are detrimental as they cause shunting in thin film device fabrication.

Thickness Measurement

The film thickness of solar cell materials is an important parameter in solar cell development. Thin film's properties, such as its structural, chemical, optical and device performance, are to some extent dependent on the film thickness. Chopra et al.[21] defined thin film as a material formed by the random nucleation and growth process of individually condensing/reacting atomic/ionic/molecular species on a substrate. The thickness of a film depends on its function when incorporated in a solar cell or other device structures. A thin-film semiconductor can be used either as a buffer, window or absorber material which suggests the films have different thicknesses in each case. In this paper, the ZnS films were intended for use as a buffer and a window layer in a CdS/CdTe solar cell device structure. It is important to note that the buffer layer thickness should be large enough to cover the FTO surface roughness.

Figure 8 shows the plot of estimated film thicknesses versus growth time for both theoretically and experimentally measured thicknesses of ZnS layers grown for different durations. The layer grown for 150 min deviates slightly from the normal trend, most probably due to low level of sulphur in the bath during this growth.

Film thicknesses of electrodeposited materials are usually estimated either theoretically using Faraday's equation or experimentally using instruments

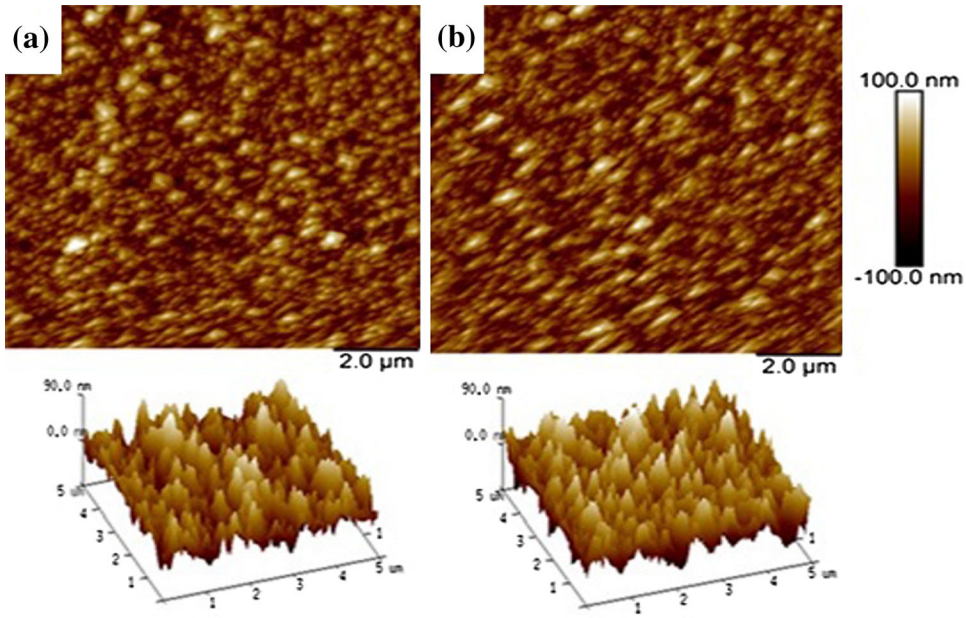

Fig. 7. Two-dimensional (2D) and three-dimensional (3D) AFM images of (a) as-deposited and (b) heat-treated ZnS layers grown on glass/FTO substrate.

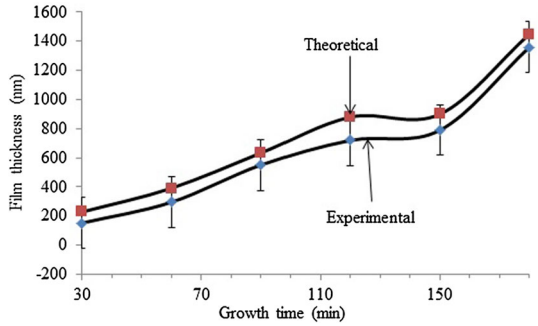

Fig. 8. Plot of theoretical and experimental thickness estimated for electroplated ZnS films.

like; an UBM Microfocus optical measurement system, dektak, SEM (cross-section), etc. In this work, the thicknesses were theoretically estimated using Faraday's equation (Eq. 2) and experimentally measured using an UBM Microfocus optical measurement system. It is observed that the film thicknesses are higher in case of the theoretically calculated values. This is due to the assumption given by Faraday in his second law of electrolysis that all the electric charge involved is used in the film deposition. However, not all electronic charge is used in the film deposition process. Part of the current is used for electrolysis of water during material deposition.[22] The theoretical estimation of the thickness was carried out using the equation,

$$T = \frac{JtM}{nF\rho}, \tag{2}$$

where T is the thickness of the film, J is the current density in mA cm^{-2}, t is the growth time, M is the molar mass of the material, n is the number of electrons transferred in the formation of 1 mol of the material (ZnS) during deposition process, F = 96,485 C mol^{-1} is the Faraday constant and ρ is the density of the material (ZnS). From Fig. 8, it is observed that film thickness increases with increase in growth time, as expected.

Electrical Resistivity Studies

The electrical property of interest here is the resistivity of the ZnS thin-film material, which is one of the most important parameters to note for thin-film solar cell fabrication. This measurement was carried out on both as-deposited and heat-treated layers using an automated I–V system at room temperature. The resistivity of ZnS under investigation was measured using a Series 2400 sourceMeter solar simulator and I–V system purchased from Lot-QuantumDesign Ltd.

The ZnS layers were found to exhibit both n-type and p-type electrical conductivities as determined by the PEC cell measurement discussed in "Photoelectrochemical (PEC) Cell studies" Section above. However, the resistivity measurement was carried out on p-type materials. Finding a suitable contact to achieve ohmic behaviour at the semiconductor/metal interface is challenging because it requires a metal with a high work function (ϕ_m) and free of Fermi level pinning effects. ZnS is known to have a low electron affinity (χ) of 3.90 eV. The appropriate

metal contact for this kind of material is gold (Au) which has a work function of 5.1 eV.[23] Prior to contact evaporation, the samples were cleaned in deionised water, dried and arranged on a mask of 2-mm diameter dots and placed inside a sputtering machine. The Au contacts were evaporated onto the material at a vacuum pressure of 10^{-3} mbar.

Several contacts from each of as-deposited and heat-treated glass/FTO/ZnS/Au structures were measured using *I–V* and the average values were taken as the resistance of each sample. This was done using two contact probes, one of the contacts connected to the FTO and the other to the Au contact. The resistivity of the film was calculated using $\rho = RA/L$, where R is the average resistance measured, ρ is the resistivity of the material, L is the thickness of the layer and A is the area of metal (Au) contacts (0.0314 cm^2). It was found that the resistivity (ρ) of the film is $\sim 6.7 \times 10^4$ Ω cm for the as-deposited and $\sim 6.9 \times 10^4$ Ω cm after heat treatment. This shows similar values in the resistivity value after heat treatment. The small increase in the resistivity value could be due to oxidation to form ZnO and/or reduction in the film thickness after heat treatment possibly due to material sublimation, thereby reducing the film thickness.

The resistivity of ZnS material obtained from different growth techniques has been reported by different researchers working on thin films and single-crystal ZnS materials. For instance, Joseph and Neville reported a resistivity value $> 10^{10}$ Ω cm[24] for their single-crystal ZnS material. Echendu et al.[6] found the resistivity of their electrodeposited ZnS films in the order of 10^4 Ω cm. A CBD ZnS thin film grown by Ubale and Kulkarni shows a resistivity on the order of 10^5 Ω cm.[25] Sadekar et al.[26] measured a resistivity of 10^6 Ω cm from solution-grown ZnS film. The variations in the value of resistivity reported by different researchers for different growth techniques could be due to variation in the film deposition conditions which may differ from one method to the other and from one grower to the other. These values are highly variable and can also be due to varying amounts of the impurities incorporated.

CONCLUSION

Successful deposition of both *n*- and *p*-type ZnS films from aqueous solution was achieved using a simple two-electrode system in a single-cell configuration. The films were characterised using most relevant selected techniques to optimise the growth conditions for thin-film solar cell application. Structural studies using XRD revealed that the materials are amorphous, as is evident from both the XRD and the SEM results. Optical absorption shows that the energy bandgap of the films are within the reported values for ZnS films (~3.70 eV). The AFM studies reveal no significant change in the film roughness after heat treatment to ~17 nm. The resistivity of the *p*-ZnS films slightly increased after heat treatment possibly due to material sublimation and/or oxidation to form ZnO during heat treatment.

ACKNOWLEDGEMENTS

We gratefully acknowledge the valuable contribution made by Hussein I. Salim, Nor Azlian Abdul-Manaf and Ayotunde Ojo in the course of writing this manuscript. The main author wishes to acknowledge the Petroleum Technology Development Fund (PTDF), Nigeria for financial support.

REFERENCES

1. T. Yasuda, K. Hara, and H. Kukimoto, *J. Cryst. Growth* 77, 485 (1986).
2. S. Tec-Yam, J. Rojas, V. Rejon, and A.I. Oliva, *Mater. Chem. Phys.* 136, 386 (2012).
3. O.K. Echendu, F. Fauzi, A.R. Weerasinghe, and I.M. Dharmadasa, *Thin Solid Films* 556, 529 (2014).
4. O.K. Echendu and I.M. Dharmadasa, *Energies* 8, 4416 (2015). doi:10.3390/en8054416.
5. O.K. Echendu and I.M. Dharmadasa, *J. Electron. Mater.* 43, 791 (2014).
6. O.K. Echendu, A.R. Weerasinghe, D.G. Diso, F. Fauzi, and I.M. Dharmadasa, *J. Electron. Mater.* 42, 692 (2013).
7. N.K. Abbas, K.T. Al-Rasoul, and Z.J. Shanan, *Int. J. Electrochem. Sci.* 8, 3049 (2013).
8. J. Han, G. Fu, V. Krishnakumar, C. Liao, W. Jaegermann, and M.P. Besland, *J. Phys. Chem. Solids* 74, 1879 (2013).
9. A. Pudov, J. Sites, and T. Nakada, http://www2.physics.colostate.edu/groups/photovoltaic/PDFs/CSU-AGU%20paper.PDF. Accessed 04/08/2015.
10. Z. Limei, X. Yuzhi, and L. Jianfeng, *J. Environ. Sci. Suppl. 21,* S76–S79 (2009).
11. A. Ates, M.A. Yildirim, M. Kundakci, and A. Astam, *Mater. Sci. Semicond. Process.* 10, 281 (2007).
12. C. Falcony, M. Garcia, A. Ortiz, and J.C. Alonso, *J. Appl. Phys.* 72, 1525 (1992).
13. A.B. Bhalerao, C.D. Lokhande, and B.G. Wagh, *IEEE Trans. Nano Technol.* 12, 996 (2013).
14. D. Peng, Z. Xi-Qing, S. Xue-Bai, Y. Zhi-Gang, and W. Yong-Sheng, *Chin. Phys.* 15, 1370 (2006).
15. I.M. Dharmadasa, A.P. Samantilleke, J. Young, and M.H. Boyle, *J. Mater. Sci. Mater. Electron.* 10, 441 (1999).
16. I.M. Dharmadasa, P.A. Bingham, O.K. Echendu, H.I. Salim, T. Druffel, R. Dharmadasa, G.U. Sumanasekera, R.R. Dharmadasa, M.B. Dergacheva, K.A. Mit, K.A. Urazov, L. Bowen, M. Walls, and A. Abbas, *Coatings* 4, 380 (2014).
17. D. Kurbatov, V. Kosyak, M. Kolesnyk, A. Opanasyuk, and S. Danilchenko, *Integr. Ferroelectr.* 103, 32 (2008).
18. J. Diaz-Reyes, R. Castillo-Ojeda, J. Martinez-Juarez, O. Zaca-Moran, J.E. Flores-Mena, and M. Galvan-Arellano, *Int. J. Circuits, Syst. Signal Process.* 8, 15–21 (2014).
19. S. Radhu and C. Vijayan, *Mater. Chem. Phys.* 129, 1132 (2011).
20. J. Tauc, R. Grigorovini, and A. Vancu, *Phys. Status Solidi.* 15, 627 (1966).
21. K.L. Chopra, P.D. Paulson, and V. Dutta, *Prog. Photovolt. Res. Appl.* 12, 69 (2004).
22. R.K. Pandey, S.B. Sahu, and S. Chandra, *Handbook of Semiconductor Electrodeposition* (New York: Allen H. Hermann, Marcel Dekker Inc., 1996).
23. O.K. Echendu (Doctoral Thesis, 106, Sheffield Hallam University, Sheffield, United Kingdom).
24. J.D. Joseph and R.C. Neville, *J. Appl. Phys.* 48, 1941 (1977).
25. A.U. Ubale and D.K. Kulkarni, *Bull. Mater. Sci.* 28, 43 (2005).
26. H.K. Sadekar, N.G. Deshpande, Y.G. Gudage, A. Ghosh, S.D. Chavhan, S.R. Gosavi, and R. Sharma, *J. Alloys Compd.* 453, 519 (2008).